PHILOSOPHICAL MAGAZINE A, 1988, VOL. 57, NO. 4, 605–620

Structural fluctuations in small particles

By J. DUNDURS

Department of Civil Engineering, Northwestern University, Evanston, Illinois, U.S.A.

L. D. MARKS and P. M. AJAYAN

Department of Materials Science and Engineering, Northwestern University, Evanston, Illinois, U.S.A.

[*Received 26 May 1987 and accepted 19 August 1987*]

ABSTRACT

We present a theoretical analysis of a phenomenon recently observed by high-resolution electron microscopy that involves rapid structural fluctuations in small f.c.c. particles below 10 nm in size. The different energy contributions to the total energy of the particle and the magnitude of the potential energy barrier between different shapes is evaluated and compared with the available energy during particle–beam interactions. The results indicate that the activation energy barrier existing between different shapes is only a few electron volts, whilst a rough estimate indicates that during electron-beam irradiation the available energy may be as much as 100–1000 eV.

§ 1. INTRODUCTION

The thermodynamic equilibrium surface morphology of individual metal particles larger than 100 nm in size is well understood in terms of the Curie–Wulff construction (Herring 1951, Linford 1973). However, as the size of the particle decreases, the theoretical predictions become less clear-cut. For instance, it has been pointed out by Hoare and Pal (1972) that a free-floating cluster containing a small number of atoms need not have a fixed structure at room temperature and can dynamically fluctuate between different shapes. In addition, the reduction in size introduces packing effects (Marks 1985 a) similar to the inclusion of complicated phenomena, such as three-body interactions (Wang, Falicon and Searchy 1984). Structural evaluations at smaller sizes based on quantum mechanical (Gordon, Cyrot-Lackman and Desjonqueres 1979) or pair-potential calculations (Allpress and Sanders 1970, Farges, de Feraudy, Raoult and Torchet 1981) have given valuable results although experimental verification is still lacking.

Recent improvements in the instrumentation of high-resolution electron microscopes have made it possible to observe small particles directly on an atomic scale (see, for example, Marks (1985 b)). It has recently been reported (Iijima and Ichihashi 1986, Smith, Petford-Long, Wallenberg and Bovin 1986) that ultrafine particles of gold (smaller than 50 Å), sitting on an amorphous substrate such as Si or SiO_2 and exposed to irradiation by an electron beam of flux 10^5 electrons $Å^{-2} s^{-1}$, change shape continually at frequencies of about 10 Hz. Real-time video recordings have allowed a detailed visual study of these dynamic fluctuations, but the different structures observed have yet to be analysed in detail. The rate of fluctuation in the above observations depends on factors such as the contact area between the particle and the

substrate, the electrical conductivity of the substrate and the energy of the incident beam. Moreover, the fluctuations are often accompanied by translational and rotational motions of the particle on the substrate (S. Iijima 1984, unpublished conference paper, 1986, private communication, A. Petford-Long 1986, private communication).

The most commonly accepted thermodynamic equilibrium form of small particles is the multiply twinned particle (MTP) structure, the details of which have been discussed by various researchers (Ogawa, Ino, Kato and Oata 1966, Ino 1967, Marks 1984, Howie and Marks 1984). It has been shown theoretically that, in most cases, MTPs are more stable than single crystals (at small sizes). The simplest model for MTPs is a combination of single-crystal tetrahedra, twin related on their adjoining faces and exhibiting discrete non-crystallographic point-group symmetries. Five such units (with two twin boundaries per single crystal unit) when put together form a decahedral MTP, or Dh, with D_{5h} symmetry, and twenty such units (with three twin boundaries per unit) form an icosahedral MTP, or Ic, with I_h symmetry. When formed from perfect single-crystal units, neither of these shapes is space filling, and they have to be distorted to form space-filling bodies. The angular deficits can be considered as 7·5° wedge disclinations; one such disclination in a Dh and six in an Ic. The distortions mentioned above introduce elastic strains into the bulk and also the surface of the particle, and these have to be considered in any realistic energy calculation. The thermodynamic stability of these MTPs has been analysed in terms of the modified Wulff construction (Marks 1984, Howie and Marks 1984) and our model here assumes a similar construction for the MTPs.

It is reasonable to assume that the various shapes during the fluid-like behaviour of small particles, which we have called quasi-melting (Marks, Ajayan and Dundurs 1986), reside on a morphological potential energy surface (Marks 1983). Local minima of this surface correspond to the observed static-particle morphologies, and the final experimental distribution depends on a thermodynamic statistical occupancy of these minima. As particles grow in size, the kinetic processes assume importance and control the structure transformations, making the fluctuations sluggish. In evaluating the magnitude of the activation energy barrier, the first step is to calculate the total energy of the particle by combining the surface energies and the elastic strain energies using a modified Wulff construction and elasticity theory. A number of different approaches can be used for the energy calculation: pair potentials (Allpress and Sanders 1970), electronic energy analyses (Gordon *et al.* 1979) or continuum models. We use the continuum model here to predict the particle morphology, although the method has limitations for smaller sizes (Marks 1985 a). Once the total energy is evaluated, the activation energy barrier is obtained as the difference between the total energy of the MTP and the energy of a single-crystal Wulff polyhedra shape for the particle.

In § 2 we present the basic model involving the fundamental unit used in the calculation with the different surface facets considered. Section 3 contains the detailed energetics including the calculation of surface energy, internal strain and surface-stress energies. A brief account of the temperature distribution existing inside the particle is also given in this section. The thermal strain energy and the interaction energy due to the thermal and elastic stresses are also evaluated but in the Appendix, since their magnitudes are negligible in comparison with the other terms and do not enter the final-energy analysis. In § 4 we present the results, and in § 5 we give a general discussion of the phenomena of small-particle fluctuations including a few possible energy-gain mechanisms during the particle–beam interaction.

§2. Model

In the earlier work (Howie and Marks 1984, Marks 1984) on the energetics of MTPs, only symmetric MTPs with all the lengths on the basic tetrahedral unit being equal were considered. This is a clear drawback since asymmetric and compound MTP structures are experimentally observed (Marks 1983). We extend this earlier model and include asymmetric shapes for the MTPs by considering an eccentric position for the disclination inside the particle. The energy is then evaluated using a continuum model in two parts: the surface energy of the particle and the elastic strain energies due to the disclination and temperature change. These two are dealt with separately.

We shall only consider here the energetics between a single crystal, a symmetrical Dh, a series of asymmetric Dh structures and a bicrystal (a particle with one twin boundary) using only ⟨111⟩ and ⟨100⟩ surface facets. A three-dimensional analysis with all possible surface facets is an intractable problem, and published results (Marks 1984, Iijima and Ichihashi 1986) show that a good approximation is achieved by considering only the ⟨111⟩ and ⟨100⟩ facets. Changes in surface facets and the motion of the 7·5° wedge disclination to the centre of the particle corresponds to a change in structure from a single crystal to a Dh, and motion to the opposite side gives a change in structure from a Dh to a bicrystal (as illustrated in fig. 1). Making use of the mirror-plane symmetry inherent in each of the segments and common to all five segments, we can say that segments two and five (see fig. 1) are identical, as are segments three and four. The general shape of the segment with different surface facets is shown in fig. 2 and is similar to the shape of a single crystal except that a (100) face which would appear along the ⟨110⟩ axis of the decahedral particle is missing. All lengths of segments are made variables, although the constraint that the segments have to match at the boundaries restricts the geometric invariance to a certain degree and simplifies the problem to a great extent.

Fig. 1

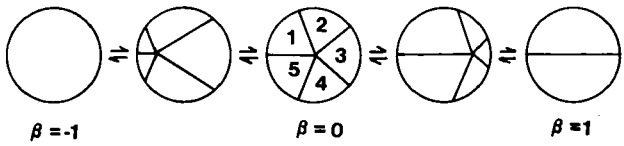

Schematic diagram showing the relation between E_w and the particle shape characterized by β.

Fig. 2

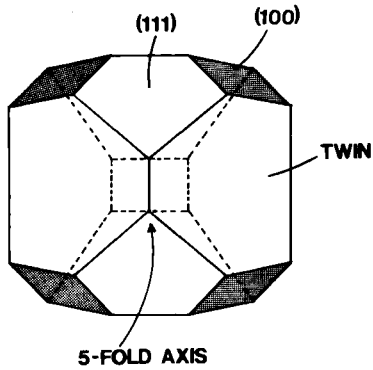

The basic tetrahedron unit showing the ⟨111⟩ and ⟨100⟩ surface facets used in the calculation.

§ 3. Energetics

3.1. *Surface energy*

The problem is to find the surface energy of the particle for a specified volume fraction of each of the five segments. This was done numerically on a VAX 780 using MINIPACK programs by evaluating the total surface and twin-boundary energies of the segment, as well as its volume, and then minimizing the dimensionless energy parameter E_w where

$$E_w = \int \frac{\gamma \, dS}{\gamma_{111} V^{2/3}}, \tag{1}$$

where V is the volume of the particle and γ_{111} the surface energy (per unit area) of a $\langle 111 \rangle$ facet. During the minimization procedure, the constraint is applied that the twin facets common to the adjoining segments are identical. This ensures that the adjoining segments match at the boundaries, and the five units fit into a complete structure. We fix the volume fraction of one of the segments and evaluate E_w as a function of this variable which in turn is expressed in terms of β, the fractional distance of the disclination from the centre. The volume fraction of 0·2 is equivalent to a value of zero for β, i.e. a symmetric decahedral particle, a volume fraction of 0·5 ($\beta = 1$) corresponds to a bicrystal with one twin boundary, whilst 0 ($\beta = -1$) is a single crystal. The value of the twin-boundary energy is set at $\gamma_t = 0{\cdot}01\gamma_{111}$, a mean value for f.c.c. metals (Howie and Marks 1984). The above calculation is repeated for three different values of the surface anisotropy ratio α or the ratio of the surface energy of a $\langle 100 \rangle$ surface to that of a $\langle 111 \rangle$ surface.

3.2. *Elasticity of the disclination*

The elastic fields of an off-centre wedge disclination in the circular region can be obtained by using the so-called slab analogy (Mindlin and Salvadori 1950). The slab analogy exploits the fact that the differential equations for the Airy stress function in plane elasticity and the transverse deflection of a thin plate loaded in bending are the same. The slab analogy also relates the boundary conditions in the two problems: to a free boundary in elasticity corresponds a clamped edge in bending. Next, noting that the singular part of the Airy stress function for the wedge disclination is of the type $[\omega\mu/\pi(\kappa+1)]r^2 \log r$ (Dundurs 1969), and $(P/8\pi D)r^2 \log r$ (where D is the flexural rigidity) for a plate loaded by a transverse concentrated force, it follows that the disclination problem can simply be solved by translating the well known Michell (1902) result for a clamped circular plate that is loaded by an eccentric force. The Airy stress function for the disclination is therefore

$$\phi = [\omega\mu/\pi(\kappa+1)][r_1^2 \log(r_1/\beta r_2) + \tfrac{1}{2}(1-\beta^2)(a^2 - r^2)]. \tag{2}$$

Apart from the symbols shown in fig. 3, ω is the angle of the wedge that is cut out of the material (positive ω corresponds to cutting out the material and closing the gap; negative ω corresponds to cutting the material and inserting a wedge of extra material), μ denotes the stress modulus and, with ν standing for Poisson's ratio, $\kappa = 3-4\nu$ for plane strain and $\kappa = (3-\nu)/(1+\nu)$ for plane stress.

Fig. 3

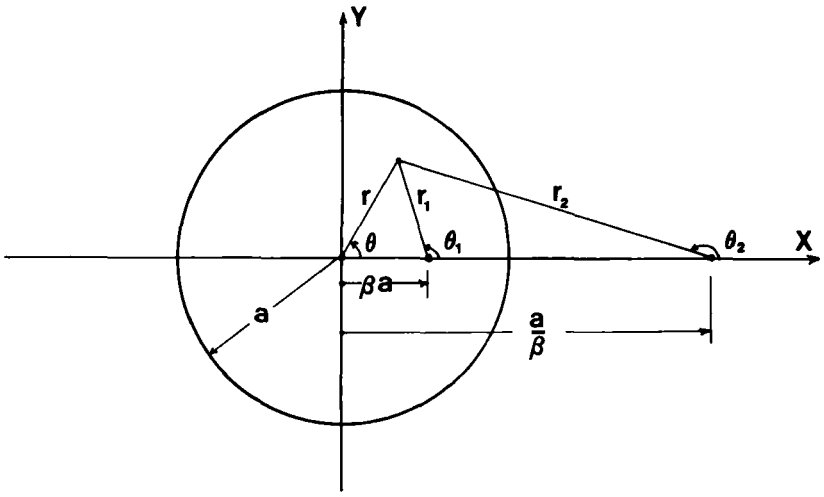

The coordinate system used for the disclination.

Relating r_1 and r_2 by the cosine law and noting that constants and terms linear in x and y are of no importance in the Airy stress function because they give zero stresses, an expanded form of (2) is seen to be

$$\phi=[\omega\mu/\pi(\kappa+1)]\{r_1^2\log r_1-r_2^2\log r_2-[2(1-\beta^2)a/\beta]r_2\log r_2\cos\theta_2 - [(1-\beta^2)^2a^2/\beta^2]\log r_2-[\log\beta+\tfrac{1}{2}(1-\beta^2)]r^2\} \quad (3)$$

which shows that ϕ consists of five simple biharmonic functions. The displacement and stress components corresponding to this Airy stress function are

$$u_x=[\omega/2\pi(\kappa+1)]\{-(\kappa+1)y(\theta_1-\theta_2)+(\kappa-1)[x\log(r_1/\beta r_2)-\beta a\log(r_1/r_2) -\tfrac{1}{2}(1-\beta^2)x]+[(1-\beta^2)a(x-a/\beta)/\beta r_2^2][2(x-a/\beta)+(1-\beta^2)a]\}, \quad (4)$$

$$u_y=[\omega/2\pi(\kappa+1)]\{(\kappa+1)(x-\beta a)(\theta_1-\theta_2)+(\kappa-1)y[\log(r_1/\beta r_2)-\tfrac{1}{2}(1-\beta^2)] +[(1-\beta^2)ay/\beta r_2^2][2(x-a/\beta)+(1-\beta^2)a]\}, \quad (5)$$

$$\sigma_{xx}=[\omega\mu/\pi(\kappa+1)]\{2\log(r_1/\beta r_2)-(1-\beta^2)+2y^2(1/r_1^2-1/r_2^2) -[(1-\beta^2)a/\beta r_2^2](2x-a/\beta-\beta a)(1-2y^2/r_2^2)\}, \quad (6)$$

$$\sigma_{xy}=[\omega\mu/\pi(\kappa+1)]2y\{-(x-\beta a)/r_1^2+(x-a/\beta)/r_2^2 -[(1-\beta^2)ay/\beta r_2^2][1-2y^2/r_2^2-[(1-\beta^2)a/\beta r_2^2](x-a/\beta)]\}, \quad (7)$$

$$\sigma_{yy}=[\omega\mu/\pi(\kappa+1)]\{2\log(r_1/\beta r_2)-(1-\beta^2)-2y^2(1/r_1^2-1/r_2^2) -[(1-\beta^2)a/\beta r_2^2][2(x-a/\beta)(1+2y^2/r_2^2)-[(1-\beta^2)a/\beta](1-2y^2/r_2^2)]\}. \quad (8)$$

Noting that, on $r=a$, $r_2=r_1/\beta$, it is easy to confirm using the given stress components that the boundary of the circular cylinder is free of tractions. Moreover, using the branch cut $0<\theta_1, \theta_2<2\pi$, in (4) and (5) puts the displacement discontinuity on the x axis to the right of disclination, and from (5)

$$u_y(x,0^+)-u_y(x,0^-)=-\omega(x-\beta a), \quad \beta a<x<a. \quad (9)$$

3.3. *Strain energy of the disclination*

It is convenient to compute the strain energy of the disclination as the work done by the tractions acting on the displacement discontinuity given by (9):

$$W^{D}=\frac{h}{2}\int_{\beta a}^{a}\omega(x-\beta a)\sigma_{yy}(x,0)\,dx, \tag{10}$$

where h is the dimension in the z direction. The details of the calculation are tedious but, when evaluated, (10) yields the surprisingly simple expression

$$W^{D}=[\omega^2\mu a^2 h/4\pi(\kappa+1)](1-\beta^2)^2=[\varepsilon_D^2\mu V/(\kappa+1)](1-\beta^2)^2 \tag{11}$$

with V denoting the volume and $\varepsilon_D=\omega/2\pi$. Thus,

$$W^{D}=W_{Dh}(1-\beta^2)^2, \tag{12}$$

where W_{Dh} is the strain energy of a symmetrical Dh, given as

$$W_{Dh}=[\varepsilon_D^2\mu V/4(1-\nu)] \tag{13}$$

by Howie and Marks (1984) for plane strain with the estimate $\varepsilon_D=0{\cdot}0205$.

It might be thought that the strain energy per unit volume for the three-dimensional case is between those for a long cylinder (plane strain) and a thin circular disc (plane stress). However, the ratio of the plane strain energy to the plane stress energy is $1/(1-\nu^2)$ which ranges only from 1 to $\frac{4}{3}$.

3.4. *Surface stress energy*

We begin by computing the hoop strain $e_{\theta\theta}$ at the boundary for the eccentric disclination. It follows from (6)–(8) that, on $r=a$, we have

$$\sigma_{xx}=[4\pi\varepsilon_D\mu(1-\beta^2)^2a^2\sin^2\theta]/\pi(\kappa+1)r_1^2, \tag{14}$$

$$\sigma_{xy}=-[4\pi\varepsilon_D\mu(1-\beta^2)^2a^2\cos\theta\sin\theta]/\pi(\kappa+1)r_1^2, \tag{15}$$

$$\sigma_{yy}=[4\pi\varepsilon_D\mu(1-\beta^2)^2\cos^2\theta]/\pi(\kappa+1)r_1^2, \tag{16}$$

where now

$$r_1^2=a^2(1+\beta^2-2\beta\cos\theta) \tag{17}$$

and $\varepsilon_D=\omega/2\pi$. From the stress transformation formula

$$\sigma_{\theta\theta}=\sigma_{xx}\sin^2\theta-2\sigma_{xy}\cos\theta\sin\theta+\sigma_{yy}\cos^2\theta, \tag{18}$$

we get

$$\sigma_{\theta\theta}=[4\pi\varepsilon_D\mu(1-\beta^2)^2/\pi(\kappa+1)](a/r_1)^2. \tag{19}$$

Hooke's law for plane elasticity gives

$$2\mu e_{\theta\theta}=\sigma_{\theta\theta}-\tfrac{1}{4}(3-\kappa)(\sigma_{rr}+\sigma_{\theta\theta}) \tag{20}$$

and, since σ_{rr} vanishes on $r=a$,

$$e_{\theta\theta}=\tfrac{1}{2}\varepsilon_D(1-\beta^2)^2(a/r_1)^2. \tag{21}$$

The average of the hoop strain on the boundary is

$$\hat{e}_{\theta\theta}=\frac{1}{2\pi}\int_0^{2\pi}e_{\theta\theta}\,d\theta. \tag{22}$$

Substituting (17) and (21), the result is

$$\hat{e}_{\theta\theta}=\tfrac{1}{2}\varepsilon_{\mathrm{D}}(1-\beta^2). \tag{23}$$

Using the approach of Howie and Marks (1984), the additional energy term due to the surface stresses can be written using the modified Wulff theory for MTPs as

$$W^{\mathrm{S}}=\hat{e}_{\theta\theta}g\gamma_{111}E_{\mathrm{w}}V^{2/3}=\tfrac{1}{2}\varepsilon_{\mathrm{D}}g\gamma_{111}E_{\mathrm{w}}V^{2/3}(1-\beta^2). \tag{24}$$

The exact value of g depends on the surface stress tensor for the material, which in turn depends on many factors such as surface impurities, surface relaxation, lattice imperfections, long- and short-range interactions between atoms (Marks 1984). For simplicity, we reform g into a semi-empirical constant and its value, in the present calculations, is taken to be of the order of unity.

3.5. *Temperature distribution*

We assume that the electron beam deposits heat throughout the volume of the particle, that heat is lost only to the substrate and that a steady state has been reached. The temperature T then satisfies the differential equation

$$\partial^2T/\partial x^2+\partial^2T/\partial y^2=-s(x,y)/k \tag{25}$$

where $s(x,y)$ is the source density (energy deposited by the electron beam per unit volume and unit time) and k denotes thermal conductivity. The particular solution of (25) for a constant source density $s(x,y)=s_0$ is

$$T=(s_0/4k)(x^2+y^2)=-(s_0/4k)r^2. \tag{26}$$

It is possible to give a simple closed solution which corresponds to an insulated boundary of the particle, with the heat removed by a sink of strength πa^2s_0 per unit thickness and placed at $x=a$, $y=0$ (fig. 4(*a*)):

$$T=T_0-(s_0a^2/k)[r^2/4a^2-\log(r_1/a)], \tag{27}$$

where T_0 is the temperature at the centre. This solution suffers from the defect, however, that it is not possible to evaluate the general temperature level because $T\to-\infty$ at the sink.

Fig. 4

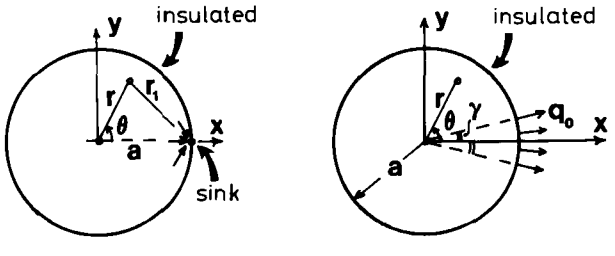

(*a*) (*b*)

Schematic diagram of the particle sitting on the substrate, used in the calculation of the temperature distribution in the particle.

Hence we must construct a solution for heat being removed on a small finite interval of the boundary (fig. 4(*b*)). The temperature distribution is taken as

$$T(r,\theta)=-\frac{s_0}{4k}r^2+A_0+\sum_{n=1}^{\infty}A_n r^n\cos n\theta \tag{28}$$

which satisfies (25). The radial component of the heat flux is $q_r=-k\partial T/\partial r$, and from (28)

$$q_r(a,\theta)=\frac{s_0 a}{2}-k\sum_{n=1}^{\infty}A_n n a^{n-1}\cos n\theta. \tag{29}$$

That part of the boundary corresponding to $\gamma<\theta<2\pi-\gamma$ is taken as insulated ($q_r=0$). There are two options for the boundary conditions on the interval $-\gamma<\theta<\gamma$ where heat is removed. One can specify a temperature distribution, say $T=0$, on the distribution of the radial heat flux. The first choice leads to a mixed boundary value problem; the solution is complicated because of the singularities at $\theta=\pm\gamma$. Hence we specify heat flux on $-\gamma<\theta<\gamma$ and for simplicity take $q_r=q_0=$constant. Expanding these boundary conditions in a Fourier cosine series on $-\pi<\theta<\pi$, and using the side condition $2\gamma a q_0=\pi a^2 s_0$ from a heat balance, we obtain

$$q_r(a,\theta)=s_0 a\left(\tfrac{1}{2}+\sum_{n=1}^{\infty}\frac{\sin n\gamma}{n\gamma}\cos n\theta\right). \tag{30}$$

Matching the coefficients in (29) and (30) yields

$$A_n=-(s_0\sin n\gamma)/k\gamma n^2 a^{n-2},\quad n=1,2,\ldots. \tag{31}$$

To find the constant A_0 in (24) we might set $T(a,0)=0$ or $\int_{-\gamma}^{\gamma}T(a,\theta)\,d\theta=0$. The first choice gives a simpler expression and, using it, the final result is

$$T(r,\theta)=\frac{s_0}{4k}(a^2-r^2)+\frac{s_0 a^2}{k\gamma}\sum_{n=1}^{\infty}\left[1-\left(\frac{r}{a}\right)^n\cos n\theta\right]. \tag{32}$$

Taking $\gamma=\frac{1}{16}$ corresponding to about 3·6°, the temperature at the centre of the particle is

$$T_0\approx 4{\cdot}0 s_0 a^2/k. \tag{33}$$

The temperature averaged over the volume of the particle is $T_0/2$. The maximum temperature of the particle for this value of γ is

$$T(a,\pm\pi)\approx 4{\cdot}5 s_0 a^2/k. \tag{34}$$

When approximate values of s_0 and k for a 25 Å gold particle are put into expressions (33) and (34), we find that the difference in the average and the maximum temperatures is only of the order of 10^{-6}°C and hence negligible. This suggests that the temperature gradients in the particle are extremely small and that the particle is not significantly heated in the process of electron-beam irradiation. This would not be the case if one encountered an anomalous value for the thermal conductivity of the particle–substrate interface, a condition which appears to be highly unlikely. The situation is further clarified by the computation of the thermal stresses and the additional energy terms, as in the Appendix.

§4. Results

As explained in the Appendix, the total strain energy is

$$W = W^{D} + W^{T} + W^{I}, \tag{35}$$

where W^{D} given by (12) is the strain energy of the disclination stresses, W^{T} that of the thermal stresses and W^{I} the interaction energy between the two fields given by (A 11) and (A 15), respectively. The most notable feature of the three terms in W is their dependence on size: $W^{D} \approx a^2 h \approx V$, $W^{I} \approx a^4 h \approx a^2 V$ and $W^{T} \approx a^6 h \approx a^4 V$. Since we are dealing here with particles with a in the range 10–100 Å, the last two terms in (35) are negligible in comparison with the first, and hence W^{D} is the only numerically important term in the result.

The results from the previous sections are represented diagrammatically in the following plots.

(1) The surface energy E_w is plotted against β for three different values of the surface anisotropy ratio α in fig. 5. For all values of α, there is a strong minimum for $\beta = 0$, or the case of the symmetrical Dh, whereas there are also shallow local minima for $\beta = +0{\cdot}5$ and $-0{\cdot}5$, indicating local stability for asymmetric shapes. As the value of α drops, the variation in E_w softens which supports the fact that MTPs are more stable for anisotropic surface energies (Howie and Marks 1984). A rise in temperature causes a decrease in surface anisotropy (since it goes to zero at the melting point) which then suggests, at this point, that the instability of small particles during electron-beam heating could be due to a thermal heating effect, if such a heating actually occurs in the particle. The addition of the strain energy term in the energetics, and the estimates of the temperature gradients existing disprove this, as will be seen later, thus

Fig. 5

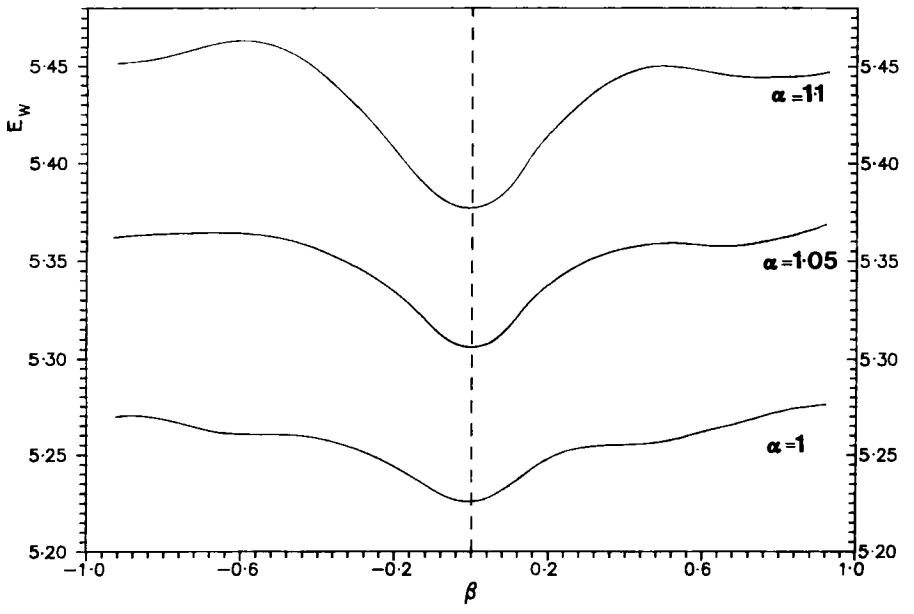

Plot showing the variation in surface energy as a function of the particle shape for three different values of the surface anisotropy ratio.

Fig. 6

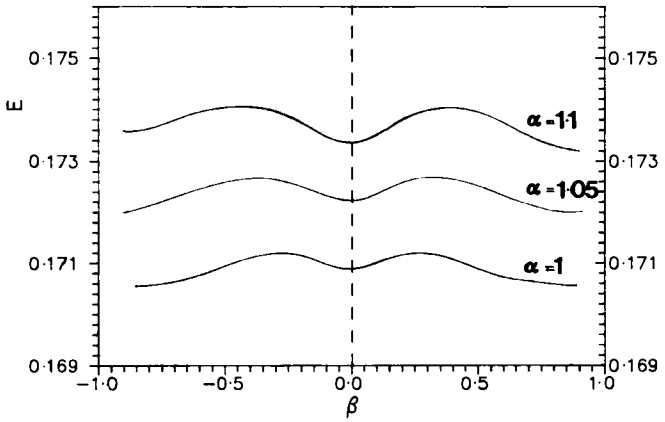

The dependence of the total energy on the particle shape after the strain energy terms are added ($R = 25$ Å).

predicting that the instability in structure is not caused by heating but is induced by other electronic phenomena.

(2) The different strain energy terms, evaluated in § 3 and the Appendix, are added to E_w and the total energy plotted against β in fig. 6. Although the strong minimum for a symmetric Dh still persists, the magnitude of the variations between $\beta = -1$ to $\beta = 1$ drops considerably. This indicates that, as we use a more realistic model including all the energy terms, the potential energy surface becomes very flat and the minimum for the symmetric Dh structure loses its significance to some extent. The local minimum is far larger than the energy difference between a Dh and single crystal, for example, and it is far more important to consider the potential energy surface than the simple energy differences. Also the difference in variations in E_w with α, as seen in the previous plot, becomes negligible and the temperature dependence of the phenomena becomes questionable. It should be noted that, among the strain energy terms, only the internal strain energy due to the disclination and the surface strain energy are important, and the other terms are negligible in magnitude when appropriate values are substituted for the constants in (35).

The solution for the temperature distribution indicates that the gradients existing in the particle are extremely small, and the particle is at almost constant temperature as it sits on the substrate. For gold on a Si/SiO_2 substrate, it follows from (33) and (34) that the difference in the magnitude of the average and maximum temperature in the particle is of the order of 10^{-6}°C. This, coupled with the result in (2) above, shows that temperature-dependent (thermal) phenomena for the instability of small particles can be ruled out.

(3) The total energy of the particle can be written in terms of an equivalent radius of the particle, which is the radius of a spherical particle having the same volume. The difference in energies between a single-crystal Wulff polyhedron and the various shapes characterized by β is plotted in electron volts against β for a 25 Å particle and $\alpha = 1{\cdot}1$ in fig. 7. The most important and fascinating observation here is the fact that the magnitude of the maximum activation barrier corresponding to the jump between the energetically most

Fig. 7

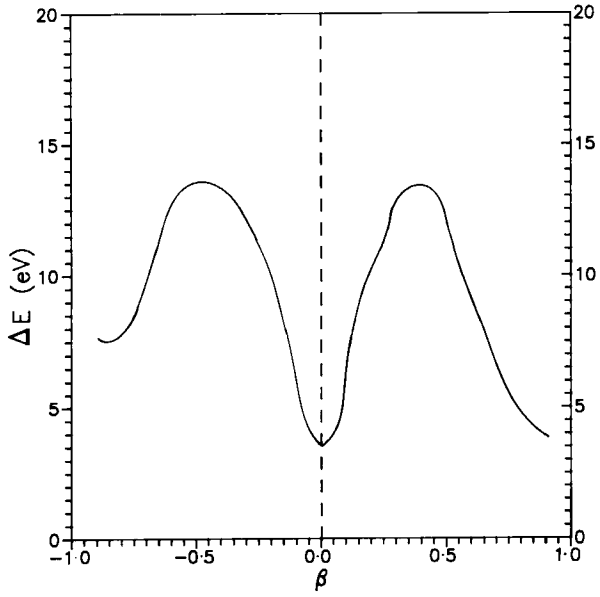

The activation energy barriers existing between a single crystal and different particle morphologies plotted against particle shape ($R = 25$ R; $\alpha = 1{\cdot}1$).

Fig. 8

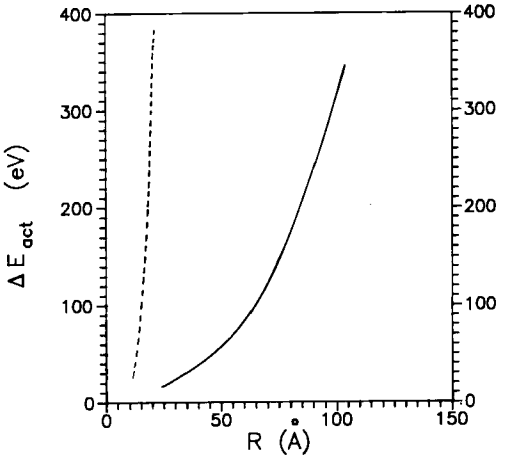

Plot of the activation energy barrier against the particle radius with the energy for melting shown by the broken curve ($\alpha = 1{\cdot}1$).

unfavourable shapes is only 10–15 eV. This indicates that a particle in the size range of 25 Å can change its structure between any of the shapes that we have considered, provided that energy of the order of 10–15 eV is available from the solid–beam interaction.

(4) The activation energy E_{act}, or the energy needed for transformation from a single crystal to any of the symmetric or asymmetric shapes is plotted against the particle radius in fig. 8. It shows that, as the particle size increases, the

activation barrier grows rapidly. In the same plot, we also show the classical energy of melting of a small particle, corrected for melting temperatures at smaller sizes (Couchman and Ryan 1978), which is seen to be several orders of magnitude larger. The relation is not simple and depends on various experimental factors, such as the nature of the substrate, the gases adsorbed on the surface of the particle and the kinetics of growth, but in any case the result supports the experimental observation that, for larger particle sizes, the fluctuations are much slower, so that the idea of a simple static-particle structure starts to reappear again.

§ 5. Discussion

The agreement between the theoretical results that we have obtained here and the experimental observations appears to be promising. The potential energy surface that we considered appears flat, and the height of the activation energy barriers existing between different shapes is only a few electronvolts (about 10 eV for a 25 Å particle) or orders of magnitude smaller than the energy required to melt the particle. The question now is how much energy is generated during the particle–beam interaction, and how much of it is available to the particle to cross the above barriers and to jump between different shapes.

We attempted an order-of-magnitude calculation to find the energy gained during the process for a 25 Å particle assuming an electron flux density of 10^5 Å^{-2} s^{-1}. First, assuming the energy deposition to be a thermal process and assuming classical mechanics for heat conduction, one arrives at an order of magnitude of 100 eV of energy generated during the interaction (the calculation also assumes a substrate temperature of 100°C, an upper bound value reported recently by Iijima and Ichihashi (1986)). However, one can also think of the energy as being transferred by electronic excitation phenomenon. Here using an electronic temperature (Buxbaum and Marks 1986), which is the temperature to which the specimen has to be heated in order to produce the same population density of a particular electronic excitation, an energy value of the order of 1000 eV is obtained. Now, this calculated energy is the intrinsic energy of the system including the atomic vibrations (thermal) and the vibrations of the lattice (phonon excitation), and only a small fraction of this is available to the particle for transformations. However, it should be emphasized that the particle needs only a small fraction of this energy, and this can clearly be considered as available.

Another important question is what the mechanism is by which the particle gains energy during its encounter with the electron beam. At first, it may seem to be a temperature-dependent effect due to simple beam heating but, as the elastic terms were added to the energy which made the surface anisotropy effect less strong and as the temperature gradients were found to be minimal inside the particle, this has ceased to be a valid reason. A second and a recent prediction is a temporal surface-charging phenomenon (Iijima and Ichihashi 1986, Howie 1986). The idea is that a core-electron excitation (Auger cascade) or secondary-electron transfer phenomena can impose Coulombic forces which can change the shapes of particles through internal atomic rearrangements. The particle or the contact area of the substrate can deviate temporarily from electronic neutrality, and this can lead to translational and rotational motions of the particle. This can be accepted as a reasonable mechanism if the particles change shape only when charged, and there is no evidence at present to believe that this is the case. Knock-on damage and surface desorption are other possibilities, but the fact that the phenomena were first observed in gold using 100 kV electrons, which is below

the damage threshold for knock-on in gold, indicates that it is not the correct mechanism. Another possibility is activation by the energy available after a core excitation (Williams 1987). However, as this yields far more energy than is required, we do not feel any need to invoke a process with a low scattering cross-section.

A reasonable answer at this point seems to be an electronic excitation phenomenon, leading to surface or bulk diffusion (Bourgoin and Corbett 1972, Knotek 1984). A Bourgoin–Corbett diffusion for the particles as a whole is a possibility. It has been experimentally observed that the fluctuations become sluggish if an electrically conducting substrate is used (S. Iijima 1986, private communication). This supports the mechanism of electronic excitation since the excited states can more readily dissipate into a conductive substrate, making the transformations slow. The actual inelastic scattering process is probably a surface or bulk plasmon mode, decaying by some as yet unclear process driving the Bourgoin–Corbett channel. As in electron-stimulated desorption processes, we can expect a very low conversion efficiency which is consistent with the relatively slow motion rates.

Although we are able to explain the dynamic behaviour of small particles on the basis of energetics, there are obvious limitations to our model. First of all, we have considered an absolutely static model with no mention of the growth kinetics. The thermodynamics becomes important only when equilibrium conditions are established after growth but, considering the fact that we are looking at a time scale in which the particles change shape without addition or removal of atoms, our results carry importance. The addition of any other facets such as $\langle 110 \rangle$ on the surface of the particle would ease the constraint on the twin boundaries, indicating that what we have found for the energy is an upper bound value. The model may break down at smaller sizes when continuum assumptions become invalid, but below a certain size there may not be enough room for the MTPs to form. Finally the energy gain mechanisms that we considered are far from comprehensive and there is still no unequivocal evidence to believe that a particular mechanism is wholly responsible for the phenomena. A detailed study remains to be done on this area.

APPENDIX

To compute the thermal stresses, we first note that, except for the single term $-(s_0/4k)r^2$ in (32), the rest of the temperature distribution is a harmonic function (it satisfies Laplace's equation $\nabla^2 T = 0$). It is known, however, that a harmonic temperature distribution gives the stresses

$$\sigma_{xx} = \sigma_{xy} = \sigma_{yy} = 0, \quad \sigma_{zz} = -E\alpha T, \tag{A 1}$$

in a simply connected cylinder with a free surface but constrained to be in plane strain (Timoshenko and Goodier 1970, p. 471). Therefore the stress components of interest can be computed easily using the formulae for a radially symmetric temperature distribution (Timoshenko and Goodier 1970, p. 445):

$$\sigma_{rr} = \frac{\alpha E}{1-\nu}\left(\frac{1}{a^2}\int_0^a Tr\,\mathrm{d}r - \frac{1}{r^2}\int_0^r Tr\,\mathrm{d}r\right) = -\frac{s_0\alpha E}{16k(1-\nu)}(a^2 - r^2) \tag{A 2}$$

$$\sigma_{\theta\theta} = \frac{\alpha E}{1-\nu}\left(\frac{1}{a^2}\int_0^a Tr\,\mathrm{d}r + \frac{1}{r^2}\int_0^r Tr\,\mathrm{d}r - T\right) = -\frac{s_0\alpha E}{16k(1-\nu)}(a^2 - 3r^2) \tag{A 3}$$

where E denotes Young's modulus. The expression for σ_{zz} is more complicated because the harmonic part of the temperature distribution enters, but it is of no immediate interest.

The strain energy of the thermal stresses is

$$W^{\mathrm{T}}=\tfrac{1}{2}\int_{\mathrm{V}}\sigma_{ij}(e_{ij}-\alpha T\delta_{ij})\,\mathrm{d}V,\quad i,j=1,2,3 \tag{A 4}$$

where e_{ij} denotes the total strain, so that the quantity inside the parentheses in (A 4) is the elastic strain. Since $e_{ij}=\frac{1}{2}(\partial_i u_j+\partial_j u_i)$ and $\sigma_{ij}=\sigma_{ji}$,

$$W^{\mathrm{T}}=\tfrac{1}{2}\int_{V}\sigma_{ij}(\partial_i u_j-\alpha T\delta_{ij})\,\mathrm{d}V \tag{A 5}$$

and, using the equilibrium condition $\partial_i\sigma_{ij}=0$,

$$W^{\mathrm{T}}=\tfrac{1}{2}\int_{V}\partial_i(\sigma_{ij}u_j)\,\mathrm{d}V-\tfrac{1}{2}\alpha\int_{V}T\sigma_{ii}\,\mathrm{d}V. \tag{A 6}$$

Next, transforming the first integral to a surface integral by Gauss's theorem,

$$W^{\mathrm{T}}=\tfrac{1}{2}\int_{S}n_i\sigma_{ij}u_j\,\mathrm{d}S-\tfrac{1}{2}\alpha\int_{V}T\sigma_{ii}\,\mathrm{d}V. \tag{A 7}$$

However, the surface integral vanishes. The side surface of the cylinder is free of tractions and $n_i\sigma_{ij}=0$. On the ends of the cylinder, $\sigma_{31}=\sigma_{32}=0$ and $u_3=0$. Therefore,

$$W^{\mathrm{T}}=-\tfrac{1}{2}\alpha\int_{V}T(\sigma_{rr}+\sigma_{\theta\theta}+\sigma_{zz})\,\mathrm{d}V. \tag{A 8}$$

This result can be simplified further because, for plane strain (Timoshenko and Goodier 1970, p. 444),

$$\sigma_{zz}=\nu(\sigma_{rr}+\sigma_{\theta\theta})-E\alpha T. \tag{A 9}$$

Thus finally

$$W^{\mathrm{T}}=-\tfrac{1}{2}\alpha(1+\nu)\int_{V}T(\sigma_{rr}^{\mathrm{T}}+\sigma_{\theta\theta}^{\mathrm{T}})\,\mathrm{d}V+\tfrac{1}{2}E\alpha^2\int_{V}T^2\,\mathrm{d}V, \tag{A 10}$$

where we have added the superscripts T on the stress components to emphasize that they are the thermal stresses.

Substituting into (A 10) the temperature from (32) and the stresses from (A 2) and (A 3), the strain energy of the thermal stresses is

$$W^{\mathrm{T}}=\frac{\pi s_0^2\alpha^2Ea^6h}{8k^2}\left[\frac{9-7\nu}{96(1-\nu)}+\frac{1}{\gamma}\sum_{n=1}^{\infty}\frac{\sin n\gamma}{n^2}+\frac{2}{\gamma^2}\sum_{n=1}^{\infty}\frac{\sin^2 n\gamma}{n^4}+\frac{4}{\gamma^2}\sum_{m=1}^{\infty}\sum_{n=1}^{\infty}\frac{\sin m\gamma\sin n\gamma}{m^2n^2}\right]. \tag{A 11}$$

Next we think of cutting the cylinder and introducing the disclination. *This operation is done with the thermal stresses present.* The cut is made on $\beta a\leqslant x\leqslant a$, $y=0$ (see fig. 3), and the disclination is induced by applying statically to the sides of the cut

the tractions that correspond to the disclination stress field. The work done on the body during this operation is

$$-\frac{h}{2}\int_{\beta a}^{a}\sigma_{yy}^{D}(x,0)[u_y^{D}(x,0^+)-u_y^{D}(x,0^-)]\,dx$$

$$-h\int_{\beta a}^{a}\sigma_{yy}^{T}(x,0)[u_y^{D}(x,0^+)-u_y^{D}(x,0^-)]\,dx, \tag{A 12}$$

where the superscripts D and T are used to distinguish the disclination and thermal deformation fields, and the displacement discontinuity in the square brackets is given by (9). The first term in (A 12) is the strain energy W^{D} of the disclination given by (12).

The second term is recognized as the interaction energy of the two fields

$$W^{I}=\omega h\int_{\beta a}^{a}(x-\beta a)\sigma_{yy}^{T}(x,0)\,dx. \tag{A 13}$$

It is clear from (A 3) that

$$\sigma_{yy}^{T}(x,0)=[s_0\alpha E/16k(1-\nu)](3x^2-a^2). \tag{A 14}$$

Substituting (A 14) into (A 13) and simplifying yields the other surprisingly simple result that

$$W^{I}=[\pi\varepsilon_{D}s_0\alpha E a^4 h/2k(1-\nu)](1-\beta^2)^2. \tag{A 15}$$

The total strain energy is the sum of W^{D}, W^{I} and W^{T}.

References

Allpress, J. G., and Sanders, J. V., 1970, *Aust. J. Phys.*, **23**, 23.

Bovin, J. O., Wallenberg, R., and Smith, D. J., 1985, *Nature, Lond.*, **317**, 47.

Bourgoin, J. C., and Corbett, J. W., 1972, *Phys. Lett.* A, **38**, 135.

Buxbaum, A., and Marks, L. D., 1986, *Proceedings of the 11th International Congress on Electron Microscopy*, Kyoto, p. 1441.

Couchman, P. R., and Ryan, C. L., 1978, *Phil. Mag.*, **37**, 369.

Dundurs, J., 1969, *Mathematical Theory of Dislocations*, edited by T. Mura (New York: American Society of Mechanical Engineers), p. 70.

Farges, J., deFeraudy, M. F., Raoult, B., and Torchet, J., 1981, *Surf. Sci.*, **106**, 95.

Gordon, M. B., Cyrot-Lackman, F., and Desjonqueres, M. C., 1979, *Surf. Sci.*, **80**, 159.

Herring, C., 1951, *Phys. Rev.*, **82**, 87.

Hoare, M. R., and Pal, P., 1972, *J. Cryst. Growth*, **17**, 77.

Howie, A., 1986, *Nature, Lond.*, **320**, 684.

Howie, A., and Marks, L. D., 1984, *Phil. Mag.*, **49**, 95.

Iijima, S., and Ichihashi, T., 1986, *Phys. Rev. Lett.*, **56**, 616.

Ino, S., 1967, *J. phys. Soc. Japan*, **27**, 941.

Knotek, M. L., 1984, *Phys. Today*, September, 27.

Linford, 1973, *Solid State Surface Science II*, edited by M. Green (New York: Marcel Dekker), p. 27.

Marks, L. D., 1983, *J. Cryst. Growth*, **61**, 556; 1984, *Phil. Mag.*, **49**, 81; 1985 a, *Surf. Sci.*, **150**, 358; 1985 b, *Ultramicroscopy*, **18**, 445.

Marks, L. D., Ajayan, P. M., and Dundurs, J., 1986, *Ultramicroscopy*, **20**, 78.

Michell, J. H., 1902, *Proc. Lond. math. Soc.*, **34**, 223.

MINDLIN, R. D., and SALVADORI, M. G., 1950, *Handbook of Experimental Stress Analysis*, edited by M. Hetenyi (New York: Wiley), p. 775.
OGAWA, S., INO, S., KATO, T., and OATA, H., 1966, *J. phys. Soc. Japan*, **21**, 1963.
SMITH, D. J., PETFORD-LANG, A., WALLENBERG, R., and BOVIN, J. O., 1986, *Science*, N.Y., **233**, 872.
TIMOSHENKO, S. P., and GOODIER, J. N., 1970, *Theory of Elasticity*, third edition (New York: McGraw-Hill).
WANG, S., FALICON, L. M., and SEARCHY, A. W., 1984, *Surf. Sci.*, **143**, 609.
WILLIAMS, P., 1987, *Appl. Phys. Lett.* (to be published).